

# *In vivo* optical imaging of CD13/APN-expression in tumor xenografts

**Angelika von Wallbrunn\***  
**Jens Waldeck\***

University of Münster  
Department of Clinical Radiology  
Waldeyerster. 1  
Haus Rosebach  
and  
Interdisciplinary Center for Clinical Research  
IZKF Münster, FG3 and ZPG 4b  
Münster, Germany NRW 48149

**Carsten Hölte**

University of Münster  
Department of Clinical Radiology  
Waldeyerster. 1  
Haus Rosebach  
and  
Department of Nuclear Medicine  
Münster, Germany NRW 48149

**Michael Zühlsdorf**

**Rolf Mesters**

University of Münster  
Department of Hematology and Oncology  
Münster Germany NRW 48149

**Walter Heindel**

University of Münster  
Department of Clinical Radiology  
Waldeyerster. 1  
Haus Rosebach  
Münster, Germany NRW 48149

**Michael Schäfers**

University of Münster  
Interdisciplinary Center for Clinical Research  
IZKF Münster, FG3 and ZPG 4b  
and  
Department of Nuclear Medicine  
Münster, Germany NRW 48149

**Christoph Bremer**

University of Münster  
Department of Clinical Radiology  
Waldeyerster. 1  
Haus Rosebach  
and  
Interdisciplinary Center for Clinical Research  
IZKF Münster, FG3 and ZPG 4b  
Münster, Germany NRW 48149

**Abstract.** The metalloexopeptidase CD13/aminopeptidase N (APN) has been shown to be involved in cancer angiogenesis, invasion, and metastasis. Therefore, a CD13/APN-targeted **NGR**-peptide was labeled with the cyanine dye Cy 5.5 and applied to image tumor xenografts with different APN-expression levels using both planar and tomographic optical imaging methods. *In vitro*, the peptide-dye conjugate showed a clear binding affinity to APN-positive HT-1080 cells, while negative MCF-7 cells and predosing with the free **NGR**-peptide revealed little to no fluorescence. *In vivo*, tumor xenografts ( $n \geq 5$ ) were clearly visualized by two-dimensional (2-D) planar fluorescence reflectance imaging (FRI) and three-dimensional (3-D) fluorescence mediated tomography (FMT) up to 24 h after injection. FMT also allowed us to quantify fluorochrome distribution in deeper tissue sections, showing an average fluorochrome concentration of  $306.7 \pm 54.3$  nM Cy 5.5 (HT-1080) and  $116.0 \pm 18.3$  nM Cy 5.5 (MCF-7) in the target tissue after 5 h. Competition with the free **NGR**-peptide resulted in a reduction of fluorochrome concentration in HT-1080 tumor tissue ( $195.3 \pm 21.9$  nM; 5 h). We thus conclude that **NGR**-Cy 5.5 combined with novel tomographic optical imaging methods allows us to image and quantify tumor-associated CD13/APN expression noninvasively. This may be a promising strategy for a sensitive evaluation of tumor angiogenesis *in vivo*. © 2008 Society of Photo-Optical Instrumentation Engineers. [DOI: 10.1117/1.2839046]

**Keywords:** optical imaging; CD13/APN; **NGR**-Cy 5.5; fluorescence mediated tomography; fluorescence reflectance imaging.

Paper 07223SSR received Jun. 19, 2007; revised manuscript received Aug. 14, 2007; accepted for publication Aug. 30, 2007; published online Feb. 25, 2008.

## 1 Introduction

Optical imaging is a desirable technique for *in vivo* cancer diagnostics since it is a highly sensitive, inexpensive imaging method that can potentially resolve relevant oncological target structures *in vivo*.<sup>1</sup> With the injection of a fluorescent compound (fluorochrome), optical imaging allows specific tagging of particular receptors, antibodies, genes, or drugs, thereby measuring compound biodistribution and pharmacokinetics and hence leading to a better understanding of these processes.<sup>1-4</sup> Combining new quantitative fluorescence imaging methods with target specific fluorochromes facilitates the visualization and quantification of specific receptor expression *in vivo*. Especially, fluorescence mediated tomography (FMT) as a newly emerging optical imaging technique has been shown to be capable of resolving fluorescence signatures three-dimensionally and quantitatively.<sup>5-9</sup>

The CD13/aminopeptidase N (APN) is a metalloexopeptidase that removes unsubstituted, N-terminal amino acids with

\*Authors contributed equally.

Address all correspondence to: Prof. Dr. Christoph Bremer, Department of Clinical Radiology, University Hospital Muenster, Albert-Schweitzer-Str. 33, D-48129 Münster, Germany. Tel.: +49-251-8345139; Fax: +49-251-8347312; email: bremerc@uni-muenster.de

neutral side chains (Ala>Phe>Leu>Gly) from peptides and amide or arylamide derivatives of amino acids.<sup>10</sup> APN has been shown to be involved in cancer angiogenesis, invasion, and metastasis.<sup>11–13</sup> A unique peptide that contains the **NGR** (asparagine-glycine-arginine)-motive binds to APN in tumor vasculature.<sup>12,14</sup> Tumor homing peptides containing the **NGR** motive, such as **CNGRC** and **GNGRG**, have been used for delivering cytokines, chemotherapeutic drugs, apoptotic peptides, and liposomes to a CD13 isoform, highly secreted on the surface of various tumor cells and tumor blood vessels.<sup>12,14–20</sup> Taking this into account, we chose a cyclic **NGR** peptide labeled with the cyanine dye Cy 5.5 for measuring and quantifying tumor homing of the conjugate with FMT, thereby comparing this technique with conventionally used fluorescence reflectance imaging (FRI) methods. Specific tumor targeting of the cyclo-[Cys-Asn-Gly-Arg-Cys]-Gly-Lys-Cy 5.5 conjugate (**NGR-Cy 5.5**) was measured on HT-1080 fibrosarcoma and MCF-7 adenocarcinoma cell assays *in vitro* and on tumor xenografts *in vivo*.

## 2 Materials and Methods

### 2.1 Synthesis and Characterization of **NGR-Cy 5.5**

Peptides were purchased as trifluoroacetate (TFA) salts in >90% purity from Bachem Distribution Services GmbH, Weil am Rhein, Germany. Cy 5.5 monoreactive NHS-ester was purchased from Amersham Biosciences Europe GmbH, Freiburg, Germany. All chemicals were used as purchased without further purification. Peptides were dissolved in aqueous bicarbonate buffer (0.1 M, pH 8.4; 1.3 mg/500  $\mu$ L) at room temperature. To this, a solution of the dye in DMSO (1.9 mg/200  $\mu$ L) was added and stirred for 60 min at room temperature in the dark. Purification was accomplished by gradient HPLC using a Knauer system with two K-1800 pumps, an S-2500 UV-detector and a RP-HPLC Nucleosil 100-5 C18 column (eluent A: water, 0.1% TFA; eluent B: acetonitrile, 0.1% TFA). Elution times were 40 to 60 min, dependent on solution quantity, at a flow rate of 1 mL/min). The product fractions were pooled, lyophilized, redissolved in phosphate-buffered saline (PBS) at 1.0 mg/500  $\mu$ L, and frozen at  $-20^{\circ}\text{C}$ . The identities of the labeled products were confirmed by high-resolution electrospray mass spectrometry (HR-ES-MS) on a QUATTRO LCZ (Waters Micromass, Manchester, United Kingdom) spectrometer with a nanospray capillary inlet,  $m/z=557.5$  [ $\text{M}$ ]<sup>3-</sup>, 837.0 [ $\text{M}+\text{H}$ ]<sup>2-</sup>. The fully assembled tracer was assessed by fluorometry and photometry for spectral characteristics (Hitachi, F-4500 fluorescence spectrometer and U-3310 UV/VIS spectrophotometer, Tokyo, Japan).

### 2.2 Cell Lines and Reagents

Human fibrosarcoma HT-1080 (ATCC: CCL-1321, Manassas, Virginia) and human adenocarcinoma MCF-7 (ATCC: HTB-22, Manassas, Virginia) cells were cultured in RPMI-1640 or MEM (Invitrogen Corporation, San Diego, California) supplemented with 10% fetal calf serum, penicillin and streptomycin (Biochrom AG, Berlin, Germany). Cells were grown routinely in a monolayer culture at  $37^{\circ}\text{C}$  in a 5%  $\text{CO}_2$  humidified air atmosphere. All antibodies were specific for CD13/APN: clone WM15 antibodies (phycoerythrin- and unconjugated)

were from Pharmingen (BD Biosciences, San Jose, California), and antibody H-300 for Western blotting and immunohistochemistry was from Santa Cruz Biotechnology (Santa Cruz, California).

### 2.3 FACS Analysis by Flow Cytometry

Cells were washed with PBS and subsequently harvested in 5 mL Versen-buffer (13.7 mM NaCl, 10 mM EDTA, 2.6 mM KCl, 8.1 mM  $\text{NaH}_2\text{PO}_4$ , and 1.4 mM  $\text{KH}_2\text{PO}_4$ , pH 7.2). Aliquots of  $2.5 \times 10^5$  cells were blocked with mouse IgG in PBS/BSA (0.1%) for 15 min at  $4^{\circ}\text{C}$ , washed twice with PBS with  $\text{Ca}^{2+}$  and  $\text{Mg}^{2+}$ , and resuspended in 150  $\mu$ L binding buffer (150 mM NaCl, 10 mM  $\text{MgCl}_2$ , 10 mM  $\text{CaCl}_2$ , 0.5 mM  $\text{MnCl}_2$ , pH 7.2, diluted 1:20 in PBS/BSA 0.1%). Antibodies (3  $\mu\text{g}/\text{mL}$ ) were added, and cells were incubated for 45 min at  $4^{\circ}\text{C}$ . Cells were washed, resuspended in PBS with 0.1% BSA, and analyzed on a Becton Dickinson FACS-Calibur (BD Biosciences, San Diego, California).

### 2.4 Western Blot

Confluent (80 to 100%) HT-1080 and MCF-7 cells were treated with 0.5 mL trypsin and harvested by scraping in cold PBS. After two centrifugation steps (1500 rpm, 5 min,  $4^{\circ}\text{C}$ ), cells were resuspended in lysis buffer [0.5% Tween 20, 50 mM Tris-HCl pH 8, 250 mM NaCl, 5 mM EDTA pH 8, 50 mM NaF, 0.5 mM  $\text{Na}_3\text{VO}_4$ , 0.9 mg/ml protease inhibitor cocktail (Sigma, St. Louis, Missouri)], and the protein concentration of each sample was determined. To concentrate the protein, a two-fold volume of cold acetone was added to each sample and placed in  $-20^{\circ}\text{C}$  for 16 h, followed by centrifugation at 10,000 g,  $4^{\circ}\text{C}$  for 30 min. Protein pellets were dissolved in 100  $\mu$ L of 6 $\times$  sodium dodecyl sulfate (SDS) sample buffer (New England Biolabs, Beverly, Massachusetts). Following precipitation, proteins were electrophoretically separated in nonreducing 10% SDS-PAGE and transferred to PVDF membranes (Millipore Corporation, Bedford, Massachusetts). After blocking, immunoblots were incubated with CD13/APN polyclonal antibody H-300 and with peroxidase-conjugated goat anti-rabbit IgG secondary antibody (Sigma, St. Louis, Missouri). Peroxidase activity was revealed using ECL chemiluminescence (Amersham, Buckinghamshire, United Kingdom) and x-ray film, as described by the manufacturers. THP-1 cell lysate (BD Biosciences, San Diego, California) was used as a positive control.

Tumor tissue was frozen in liquid nitrogen, and 0.1 to 0.5 g of each tissue was homogenized by ultrasound using an Ultra-Turrax T8 (IKA-Labortechnik, Staufen, Germany). The homogenate was resuspended in 300  $\mu$ L lysis buffer, additionally sonicated twice at 20 kHz for 5 s, and centrifuged for 30 to 60 min at 10,000 g to remove cell debris. The supernatant was taken for determining protein concentration following SDS-PAGE and Western blotting.

### 2.5 Aminopeptidase N Activity Assay

Surface aminopeptidase activity of intact cells was measured by plating 5000 cells/well in a 96-well plate (Lumox-Multiwell, Greiner Bio-One GmbH, Frickenhausen, Germany). Cells were allowed to recover for 24 h, followed by washing with PBS and incubating with 100  $\mu\text{M}$  L-alanine-4-methyl-7-coumarinylamide-(MCA)-trifluoroacetate (Fluka) in

PBS with 0.5% BSA and 20 mM HEPES (pH 7.2).<sup>21</sup> The release of fluorescent product 7-amido-4-methylcoumarin was monitored on a Kodak Gel Logic 200 Imaging System (Kodak, New Haven, Connecticut), with  $\lambda_{\text{exc}}$  of 360 nm and  $\lambda_{\text{em}}$  of 460 nm after 90 min. To assay for inhibition of enzymatic activity due to binding of CD13-specific antibody WM15 or the **NGR**-peptide, cells were pretreated in PBS containing an excess of antibody (5  $\mu\text{g}/\text{mL}$ ) or peptide (25  $\mu\text{g}/\text{mL}$ ) at 37°C for 1 h.

## 2.6 *In Vitro* CD13/APN Ligand Binding Studies

Cells were seeded in 24-well plates and incubated in culture medium overnight. For binding studies, cells were washed twice with PBS and resuspended in 150  $\mu\text{L}$  cation-buffer diluted 1:20 in PBS/BSA (0.1%). Cy 5.5 (up to 30  $\mu\text{M}$ ) or **NGR**-Cy 5.5 (12.5  $\mu\text{M}$ ) was added into each well. After an incubation period of 1 h at 37°C, cells were washed twice with PBS and resuspended in binding buffer. For blocking studies, free **NGR**-peptide (125  $\mu\text{M}$ ) was added to each well for 45 min at 37°C. Cells could be directly visualized by fluorescence microscopy (40 $\times$  objective magnification, Nikon TE 2000-S, Tokyo, Japan). The microscope was equipped with a mercury vapor lamp, 620/775 nm and 545/675 nm (excitation/emission) filters (AHF Analysentechnik, Tuebingen, Germany), a Nikon DXM1200F camera, and ACT1/DXM1200F software (Nikon, Tokyo, Japan).

## 2.7 Immunohistochemistry

Tumors were removed and embedded in buffered formalin (4%, pH 7.0). Immunohistochemistry has been carried out commercially by Habedank-LID (Berlin, Germany) using the specific anti-CD13mAb H-300. For the *in vivo* visualization of **NGR**-Cy 5.5 uptake in tumor tissue, tumors were removed 24 h p.i., embedded in Tissue-Tek O.C.T. (Sakura, Zoeterwoude, Netherlands), snap-frozen, and serial-sectioned (10  $\mu\text{m}$ ). After drying, tissue fluorescence was evaluated by fluorescence microscopy.

## 2.8 Tumor Xenografts

All animal studies were approved by the institutional review boards (# G76/2005). Female athymic nude mice (*nu/nu*) were obtained from Charles River Laboratories (Sulzfeld, Germany). At 4 to 6 weeks of age,  $3 \times 10^6$  HT-1080 or MCF-7 cells suspended in 100  $\mu\text{L}$  PBS and Matrigel (BD Biosciences, San Diego, California) were injected subcutaneously in the flank and thoracic wall, respectively. When tumors reached 4 to 6 mm in diameter, the tumor-bearing mice were anesthetized by an i.p. injection of ketamine (125 mg/kg bw) and xylazine (12.5 mg/kg bw) and subjected to *in vivo* imaging studies.

## 2.9 *In Vivo* Optical Imaging Systems – Fluorescence Reflectance Imaging

The combination of x-ray and optical fluorescence reflectance imaging (FRI) was performed using the Image Station In Vivo FX Imaging System (Kodak Molecular Imaging Systems, New Haven, Connecticut), which is equipped to provide multiwavelength fluorescence, luminescence, x-ray, and radioisotopic imaging. Fluorescence is provided by a 150-W halogen illuminator with selectable bandpass excitation and emission

filters. For Cy 5.5 excitation,  $625 \pm 18$  nm and emission  $700 \pm 17.5$  nm were employed. X-ray energy is provided by a 35-Kvp, 150- $\mu\text{amp}$ , microfocus source in an enclosed chamber above the animal. A specialized radiographic phosphor screen is moved into the imaging path under the animal, which transduces the x-ray energy to light. Light from the fluorescence and/or the radiographic screen is captured with the 4-million-pixel cooled CCD camera equipped with a 10 $\times$  zoom lens. Images were captured 1, 3, 5, and 24 h after probe injection. Image acquisition times were 30 s per animal at the emission wavelength. Optical images were co-registered with x-ray background images, and regions of interest were selected and analyzed with the Kodak MI 4.0 software.

## 2.10 Fluorescence Mediated Tomography

All tomographic optical imaging studies were performed with a small-animal fluorescence mediated tomography (FMT) system from VisEn Medical, Inc. (Woburn, Massachusetts) that has been described in detail elsewhere.<sup>6</sup> The central piece of the system is the animal-imaging chamber configured in a parallel plate geometry. The chamber is scanned by a movable optical fiber that can excite a user-defined matrix of typically 50,000 to 100,000 source-detector projection pairs. The light source is software-selectable from two high-power laser diodes at 670 nm and 745 nm, operating in the range of 5 mW to 150 mW. Detection is performed with a thermoelectrically cooled CCD camera by means of an imaging lens and appropriate bandpass filters (three-cavity interference at 675 nm or 755 nm for excitation measurements, and 705 nm or 770 nm for emission measurements). Tomographic reconstruction is based on the normalized Born approximation, a diffraction optical tomographic technique that uses a diffusion-type theoretical photon propagation model in biological tissue. The underlying assumption of the mathematical model has been propagation in a homogeneous diffuse medium with average optical absorption and scattering properties those of small rodents at the relevant wavelengths. However, it has been demonstrated that because of the appropriate data normalization scheme applied, the algorithm is very accurate even in highly heterogeneous media and *in vivo*.<sup>5</sup> The instrument is calibrated on each channel using euthanized mice with surgical implants of known fluorochrome concentration and is able to recover fluorescence depth, size, and concentration in three dimensions from tissue at any depth. The system exhibits strict linearity over a broad range of biologically relevant concentration and detection sensitivities in the order of femtomoles.<sup>22</sup> Animal scan times are in the range of 2 to 5 min; tomographic reconstruction times on a standard desktop PC are about 1 to 3 min.

For *in vivo* experiments, 2 nmol **NGR**-Cy 5.5 were injected into the tail vein of each mouse ( $n=5$  for MCF-7,  $n=6$  for HT-1080 xenografts). FRI and FMT were performed 1, 2, 5, and 24 h (FRI additional 5, 10, and 30 min) post injection. Blocking studies were accomplished by injecting 10 mg/kg **NGR**-peptide in 100  $\mu\text{L}$  PBS (200 nmol) 10 min before injection of the labeled peptide ( $n=6$  for HT-1080 xenografts). For biodistribution studies, FRI images of isolated organs (tumor, muscle, heart, spleen, kidney, liver, and lung) were carried out 24 h after injection of the tracer.

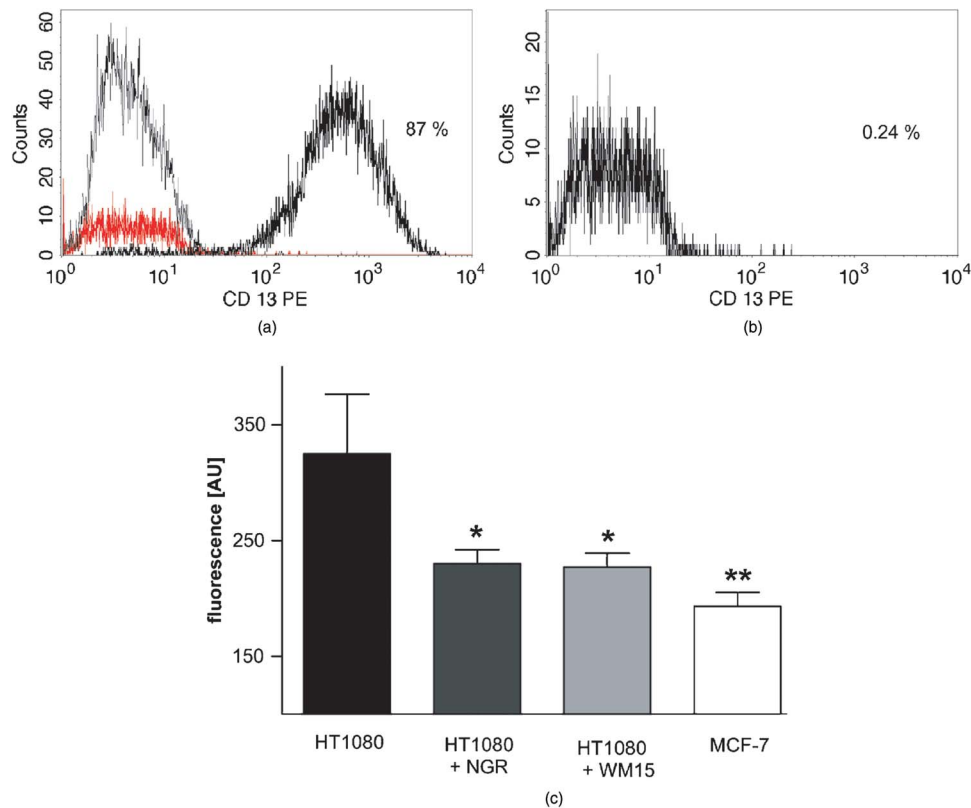


**Fig. 1** Expression of CD13/APN *in vitro*. Human HT-1080 [(a), black curve] and MCF-7 [(a), red curve, which is enlarged in (b)] carcinoma cells were analyzed by flow cytometry using monoclonal antibody WM15-PE (CD13/APN specific) or isotype control (mouse-IgG1-PE). The results are presented in histograms (i.e., distribution of cells according to their fluorescence intensity). Numbers indicate the percentage of cells that were CD13/APN positive. (c) APN activity assay using L-alanine-4-methylcoumarinylamide-(MCA)-trifluoroacetate as substrate. The release of fluorescent product 7-amido-4-methylcoumarin was monitored on positive HT-1080 fibrosarcoma and negative MCF-7 adenocarcinoma cells. To assay for inhibition of enzymatic activity, binding of CD13-specific antibody WM15 and the **NGR**-peptide was measured on HT-1080 cells. (Color online only.)

### 2.11 Statistical Analysis

Data are presented as mean  $\pm$  SEM (standard error of the mean). Statistical analysis of *in vivo* tumor fluorescence was conducted using a two-tailed, unpaired student t-test. A p-value  $\leq 0.05$  was considered to be significant.

## 3 Results

### 3.1 Synthesis and Characterization of **NGR**-Cy 5.5

The NHS ester of the near infrared fluorophore Cy 5.5 is reacted with an equimolar amount of the cyclo-[Cys-**Asn**-Gly-Arg-Cys]-Gly-Lys (**NGR**) peptide and purified by reversed phase HPLC (purity  $\geq 95\%$ ). The retention time was 28.5 min. Yields of the **NGR**-Cy 5.5 conjugate were typically 75 to 90%, as calculated with  $\epsilon_{675} = 250,000 \text{ (mol/L)}^{-1} \text{ cm}^{-1}$  from the absorption spectra measured with the PBS solution. The excitation and emission spectrum of the targeted probe remained unchanged as compared to the nonmodified fluorophore showing excitation and emission peaks at 675 nm or 694 nm, respectively.

### 3.2 CD13 Protein Expression in HT-1080 and MCF-7 Cells

To determine the cellular origin of the CD13/APN receptor and its activity in HT-1080 and MCF-7 cells, cell lines were

analyzed for CD13 protein expression by FACS, Western blot, and immunohistochemistry as well as by measurement of the specific aminopeptidase activity. For flow cytometry, cells were incubated with PE-labeled WM15 antibody directed against the human APN, and binding was analyzed (Fig. 1). Approximately 87% of the HT-1080 cells expressed the APN-receptor. In contrast, the receptor was hardly detected on MCF-7 adenocarcinoma cells [0.24%; see also Fig. 1(b)]. CD13 Western blotting of HT-1080 and MCF-7 cells and tumor tissues with the H-300 antibody, recommended for detection of CD13 of mouse, rat, and human origin, confirmed the apparent  $M_r$  of APN at 150,000. THP-1 cell lysate was used as a positive control. The APN enzyme was expressed only on HT-1080 cells and tumor tissue, while MCF-7 cells and tumors are negative for CD13 expression (not shown). Proper catalytic function of the CD13 protein was verified using a specific neutral aminopeptidase activity assay [Ref. 23; Fig. 1(c)]. CD13 activity in HT-1080 and MCF-7 cells is correlated with the expression measured by flow cytometry and Western blot analysis. The enzyme activity in HT-1080 cells could be specifically blocked by the WM15 antibody<sup>24</sup> and the **NGR**-peptide.

### 3.3 *In Vitro* **NGR** Binding Assays

Based on the CD13 protein expression data, the binding prop-

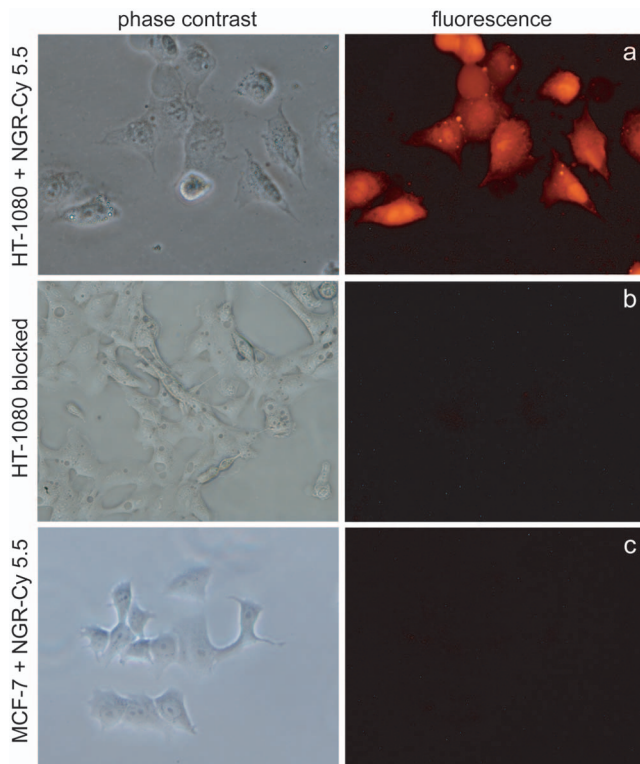


**Fig. 2** Binding affinity of **NGR-Cy 5.5** to tumor cell lines with different CD13/APN expression level. HT-1080 fibrosarcoma cells [(a) and (b)] and MCF-7 adenocarcinoma cells (c) were incubated with 12.5  $\mu\text{M}$  **NGR-Cy 5.5** to assess the target affinity of the probe. In accordance with FACS analysis and Western blot data, HT-1080 cells producing high CD13/APN levels revealed strong cellular fluorescence [(a): fluorescence microscopy; left: phase contrast], which could be selectively blocked by coincubation with the unlabeled **NGR**-peptide (b). MCF-7 cells (c), which lack CD13 expression, did not bind the targeted fluorochrome (objective magnification: 40 $\times$ ).

erties of cyclo-[Cys-Asn-Gly-Arg-Cys]-Gly-Lys-Cy 5.5 (**NGR-Cy 5.5**) to the cell lines were evaluated by fluorescence microscopy (Fig. 2). Negligible signals were detected when cells were incubated with the nonmodified Cy 5.5 dye alone (up to 30  $\mu\text{M}$ ; data not shown), and also for MCF-7 cells following incubation with up to 12.5  $\mu\text{M}$  of the labeled tracer [Fig. 2(c)]. The labeled peptide bound distinctly to HT-1080 cells [Fig. 2(a)]. The fluorescence was distributed over the cell surface and membrane-associated. Blocking of the signal was possible with a tenfold excess of unlabeled **NGR**-peptide [125  $\mu\text{M}$ ; Fig. 2(b)].

### 3.4 Immunohistochemistry

Immunohistochemistry on tumor tissue slides with CD13 antibody H-300 [Figs. 3(c) and 3(d)] exhibited membranous CD13/APN antigen expression on HT-1080 cells and only background staining in MCF-7 xenografts. Specific *in vivo* binding of **NGR-Cy 5.5** in HT-1080 tumor tissue could be visualized in Fig. 3(e), exhibiting an intense, membranous fluorescence in tumor tissue 24 h after injection of the optical tracer, whereas MCF-7 tissue showed only background staining [Fig. 3(f)].

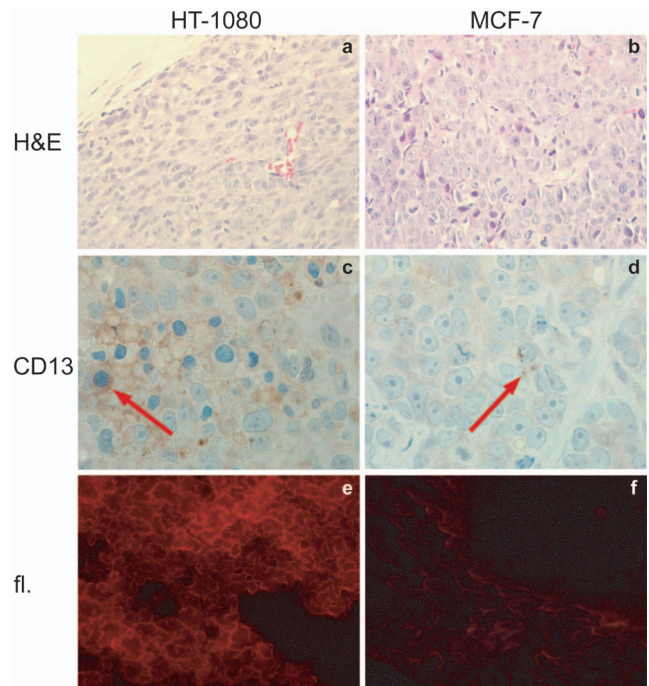


**Fig. 3** *In vivo* expression of CD13/APN in tumor xenografts. Immunohistochemical staining of CD13/APN and fluorescence microscopy of tumor slides taken 24 h after injection of **NGR-Cy 5.5**. Paraffin sections from HT-1080 and MCF-7 tumor xenografts were stained with: H&E [(a) and (b)] and CD13 [(c) and (d); H-300; 5  $\mu\text{g}/\text{ml}$ ]. Nuclei were counterstained with hematoxylin. HT-1080 tumors exhibited a strong, membranous CD13 expression (c), whereas MCF-7 tumors showed only background CD13 staining (d). Red arrows exemplify CD13 staining. HT-1080 tissue sections (e) exhibited a strong cellular fluorescence indicating a high binding of the optical tracer, while MCF-7 tissue showed only background staining. Objective magnification 20 and 40 $\times$ .

### 3.5 *In Vivo* Target Assessment and Optical Imaging

Figure 4(a) shows typical NIR fluorescence reflectance images of mice with HT-1080 ( $n=6$ ) and MCF-7 ( $n=5$ ) tumors, respectively, 24 h after injection with **NGR-Cy 5.5**. After clearing of the unbound circulating fluorochromes, the HT-1080 tumor xenografts could be clearly delineated from the surrounding background tissue up to 24 h with maximal fluorescence intensities of  $2756.2 \pm 209.4$  AU, visible 3 h post injection [Fig. 4(b)]. Compared to the targeted probe, the blocking experiment revealed lower fluorescence intensities (e.g., 1 h post injection:  $2339.3 \pm 269.9$  AU versus  $1999.5 \pm 213.5$  AU;  $n=6$ ;  $p < 0.05$ ). Target-to-background ratios (TBR) after tracer injection ranged around  $1.61 \pm 0.52$  ( $1.54 \pm 0.56$  for the blocking experiment). MCF-7 xenografts showed a weaker fluorescence, indicating a lower expression of the CD13/APN receptor [ $1407.5 \pm 122.0$  AU 3 h p.i.; Fig. 4(b)]. In HT-1080 tumor xenografts, the nonmodified Cy 5.5 revealed a fluorescence intensity of  $1404.4 \pm 243.8$  AU ( $n=7$ ) 24 h post injection (data not shown).

FMT confirmed the FRI results, exhibiting a strong fluorochrome distribution in the target tissue throughout the tumor (Fig. 5). Quantitative data analysis revealed a fluorochrome concentration 5 h after injection of  $306.7 \pm 54.3$  nM **NGR-Cy 5.5** (Fig. 5), while blocking with the free peptide

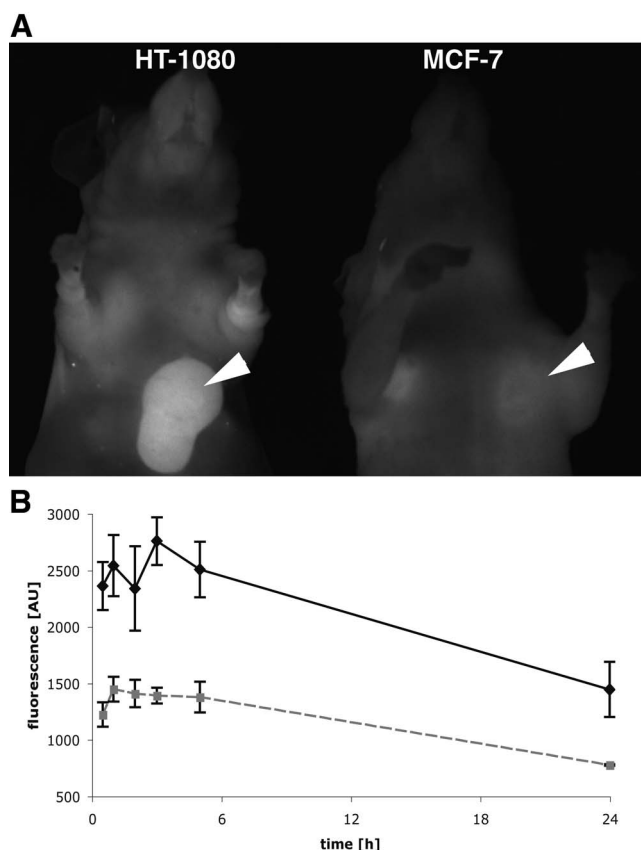


**Fig. 4** *In vivo* fluorescence reflectance imaging of HT-1080 and MCF-7 xenografts. HT-1080 fibrosarcoma ( $n=6$ ) and MCF-7 adenocarcinoma ( $n=5$ ) bearing mice were i.v. injected with the **NGR**-Cy 5.5 probe and imaged the following 24 h using a multichannel fluorescence reflectance imager (FRI). (a) FRI image 24 h past **NGR**-Cy 5.5 injection. Tumors were marked with an arrow. (b) The fluorochrome showed a strong retention over the time into the tumor (solid line), revealing a significantly higher target to background ratio as compared to APN-negative MCF-7 xenografts (dashed line). Tracer uptake could be blocked by preinjection of the unlabeled peptide (not shown).

resulted in an average fluorochrome concentration of  $195.3 \pm 21.9$  nM **NGR**-Cy 5.5 (Fig. 5). TBR values for this time-point ranged around  $7.53 \pm 4.04$  and  $3.33 \pm 2.13$  for the blocking experiment. Tumor fluorescence reached maximum intensities after 5 h and showed a slow clearance over the time [Fig. 5(g)]. Fluorochrome concentrations in nontarget tissue were significantly lower and ranged around  $116.0 \pm 18.3$  nM.

### 3.6 Biodistribution

The distribution of Cy 5.5-labeled **NGR**-peptide was measured in tumor, muscle, heart, lung, spleen, kidneys, and liver from nude mice bearing HT-1080 fibrosarcoma ( $n=6$ ) and MCF-7 adenocarcinoma ( $n=5$ ) tumors. Data were obtained by FRI measuring 24 h post injection of the tracer. A representative example of **NGR**-Cy 5.5 biodistribution in HT-1080 tumor-bearing mice is shown in Fig. 6. The highest concentration of optical tracer 24 h after injection was determined in kidneys ( $792.6 \pm 272.6$  AU for HT-1080 and  $725.3 \pm 52.6$  AU for MCF-7), followed by the accumulation

in liver ( $398.0 \pm 86.9$  AU), tumor ( $331.9 \pm 151.7$  AU), and lung ( $306.5 \pm 38.6$  AU). Preinjection of the unlabeled peptide resulted in decreased uptake in all dissected tissues (data not shown).

## 4 Discussion

Targets that are located on the endothelial surface are ideal candidates for *in vivo* molecular imaging approaches because pharmacological barriers are virtually nonexistent. CD13/APN is an ectoenzyme located in the outer cell membranes of various cells like epithelial cells, macrophages, and endothelial cells. Therapeutic targeting of the CD13/APN receptor has successfully been performed using, e.g., **NGR**-fusion peptides with related anticancer prodrugs exhibiting selective cytotoxicity toward CD13/APN positive tumor cells or angiogenic endothelial cells.<sup>14,15,18,24–26</sup> More recently, fluorochrome labeling of **NGR**-peptides has been shown to be feasible.<sup>17</sup>

For our study, we chose a cyclic **NGR**-peptide with a cystin group and a gly-lys carboxy terminus as a spacer function. The use of a cystin moiety for cyclization was chosen because of the reported enhanced tumor targeting efficiency of such peptides.<sup>15</sup> CD13/APN activity of positive HT-1080 cells<sup>16</sup> and negative MCF-7 cells were demonstrated by FACS, Western blotting, and an APN activity assay using Ala-MCA as substrate. Blocking of CD13-specific aminopeptidase activity with the **NGR**-peptide and the peptide-dye conjugate was in line with the activity-blocking antibody WM15,<sup>23,24</sup> indicating the specific binding of the labeled **NGR**-peptide to the target structure.

In *in vitro* binding studies evaluated by fluorescence microscopy, the peptide-dye conjugate showed distinct binding affinity to HT-1080 cells, while MCF-7 cells and incubation of cells with Cy 5.5 revealed little to no fluorescence. Initially, the fluorescence was membrane associated – a phenomenon also observable in fluorescence microscopic analysis of the tumor xenografts; prolonged incubation times resulted in endocytosis of the tracer and nuclear staining. The specificity of the probe could be confirmed by a competition assay with a tenfold excess of unlabeled **NGR**-peptide, which resulted in a reduction of cellular fluorescence. Thus, *in vitro* tracer binding results closely correlate with FACS and APN activity assays and suggest a high binding affinity of the peptide-dye conjugate to the target.

*In vivo*, HT-1080 xenografts were clearly visualized by FRI up to 24 h after i.v. injection of **NGR**-Cy 5.5, showing a maximum TBR of  $1.61 \pm 0.52$  after 1 h. Blocking with free peptide resulted in a decreased uptake of the optical tracer (TBR  $1.54 \pm 0.56$ ). MCF-7 tumors showed a TBR of  $0.96 \pm 0.23$ . To overcome FRI-related quantification problems, FMT was performed in a group of animals, allowing the three-dimensional (3-D) reconstruction and quantification of fluorochrome distribution *in vivo*. At maximum tumor tracer uptake after 5 h, FMT data correlates nicely with *in vitro* and FRI data, reflecting the different APN cellular expression level for HT-1080 and MCF-7 tumors. Blocking with the unlabeled peptide led to a decreased uptake of optical tracer (e.g., for HT-1080 after 24 h  $112.8 \pm 25.7$  nM). Besides target-specific fluorochrome accumulation, nonspecific accumulation of the tracer occurs due to perfusion and vascular permeability effects as well as endocytosis of the peptides

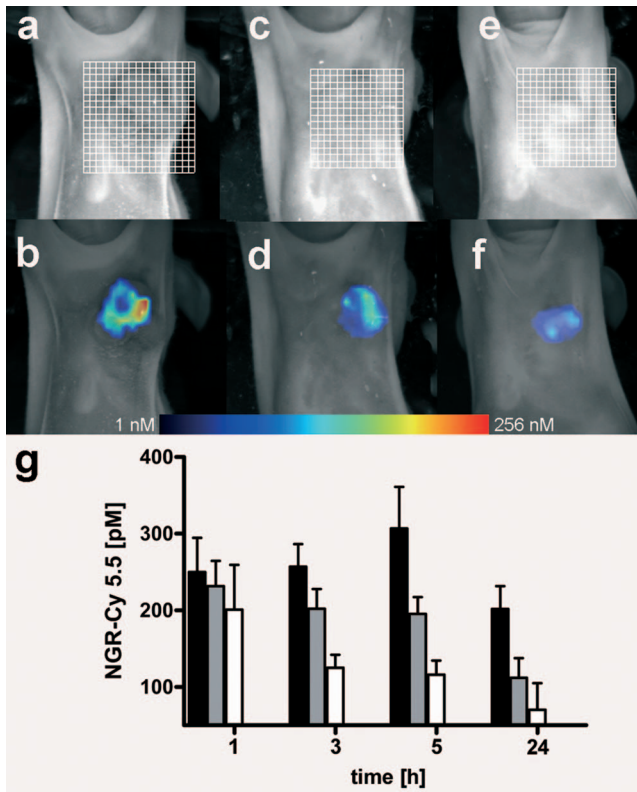


**Fig. 5** Fluorescence-mediated tomography of HT-1080 and MCF-7 tumor bearing nude mice. FMT experiments were performed to visualize and quantify the three-dimensional (3-D) fluorochrome distribution in deeper tissue sections. The fluorochrome concentration is displayed color encoded (scale: 1 to 256 nM). FMT was carried out 24 h after injection of 2 nmol **NGR-Cy 5.5** probe in HT-1080 (a) and MCF-7 (e) tumor-bearing nude mice. In order to assess probe specificity, 200 nmol of the unlabeled peptide were i.v. injected 10 min before application of the **NGR-Cy 5.5** probe (c). FMT revealed intense fluorochrome retention 60 min after probe injection in HT-1080 tumors (b), which could be significantly reduced after pretreatment with the nonmodified peptide (d). Compared to the fluorescence measured in HT-1080 tumors, the fluorochrome accumulation in MCF-7 tumors (f) was substantially lower. Tumor fluorescence washout over the time was slower in HT-1080 than in MCF-7 tumor tissue (g), black bar = native HT-1080; grey bar = blocked HT-1080; white bar = MCF-7.

over time. This effect was also observed here by imaging the nonmodified fluorophore and has been described previously for other non-target-specific NIR-fluorochromes.<sup>27</sup> These non-specific, contrasting mechanisms can also explain the relatively high remaining fluorescence signal after blocking with the free peptide. Necrotic areas within the tumor also lead to a heterogeneous tracer uptake and will influence the correlation between **NGR-Cy 5.5** and APN expression. TBR measured by FMT for HT-1080 xenografts (e.g., 5 h post injection  $7.53 \pm 4.04$ ) was significantly higher as compared to corresponding FRI data ( $1.61 \pm 0.52$ ). This may be on one hand attributed to a lower amount of bleed-through between the excitation and emission spectrum in the FMT. On the other hand, this demonstrates the capability of resolving and differentiating deeply located tissue fluorescence (e.g., deriving from the liver) from more superficially located tumor-associated fluorochrome accumulation. While FRI cannot differentiate between deeply located, strongly fluorescent organs (e.g., liver) and superficial fluorochrome tumoral accumulation, cross-sectional imaging with FMT can. Thus, scattered fluorescence from deep-seated structures can significantly spoil the TBR in FRI compared to FMT.

Direct imaging of excised organs 24 h p.i. exhibited a high accumulation of the optical tracer not in the tumor but in the kidneys and liver of all tested mice. That has a lot to commend a rapid blood clearance and a renal excretion of the **NGR-Cy 5.5** peptide, a feature that is preferable for further clinical applications. Nevertheless, CD13 expression by the reabsorptive epithelium of the kidney was also reported,<sup>28,29</sup> but **NGR** drug conjugates like **NGR-TNF** failed to bind to CD13 expressed in normal kidney,<sup>24</sup> indicating a selective tumor-homing property to a specific CD13 isoform. Further studies are necessary to clarify the binding properties of **NGR**-conjugated optical imaging probes to different APN isoforms. However, the immunohistochemical data suggest that the **NGR-Cy 5.5** probe binds to both the membrane-associated protein of the tumor cells as well as endothelial targets.

For *in vivo* applications, specifically for tomographic imaging in deep tissue sections, a maximum TBR is desirable.

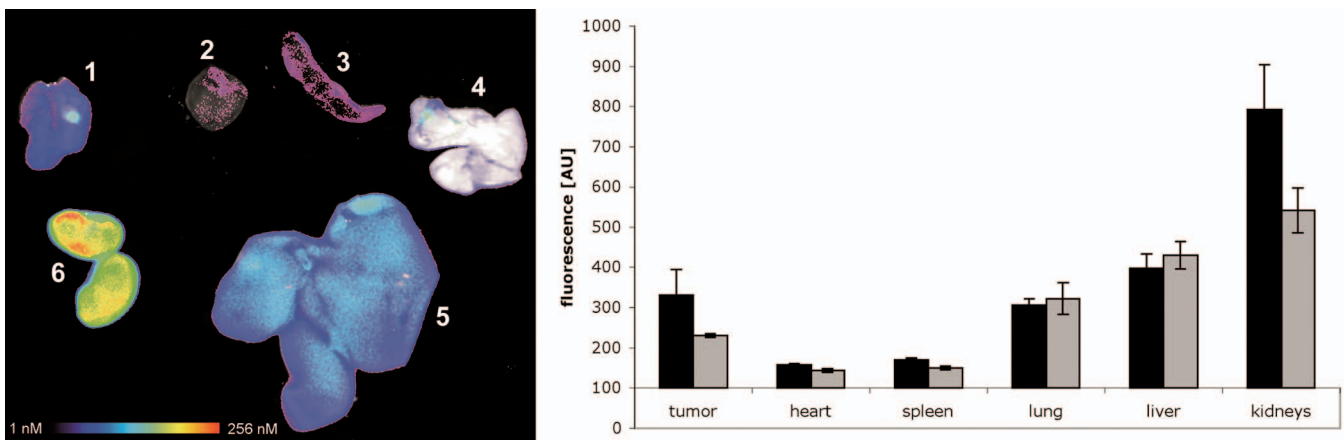


**Fig. 6** Representative overlay of white light and color-encoded FRI images of dissected organs of HT-1080 tumor-bearing nude mice. Animals ( $n=6$ ) were sacrificed 24 h after intravenous injection of 2 nmol **NGR-Cy 5.5**. Enhanced fluorochrome accumulation was detected in kidneys, liver, and lung tissue [(1): HT-1080 tumor, (2) heart, (3) spleen, (4) lung, (5) liver, (6) kidneys], indicating a high tracer washout of liver tissue and a renal excretion. The fluorochrome concentration is displayed color encoded (scale: 1 to 256 nM).

The affinity of the currently available **NGR-NIR-dye** conjugate is moderate. Different strategies have been proposed for other peptidic tracers, especially the RGD-peptide directed against the integrin  $\alpha_v\beta_3$ -receptor, to increase the target affinity of the imaging agent and decrease a high accumulation in other organs such as liver and kidneys. Possible methods are glycosylation of the tracer, peptide carbohydrate conjugates, and peptidomimetics based on the **NGR**-structure as well as heterodimeric, homodimeric, and homotetrameric ligand systems as tested for the RGD-peptide.<sup>30–32</sup> These modifications have already been carried out with radio-labeled<sup>30,33</sup> and Cy 5.5-labeled RGD probes.<sup>34</sup> The results could be a useful source for the development of **NGR** optical imaging probes.

A clinical translation of this optical imaging technology is conceivable for certain organs such as breast or head and neck tumors. The feasibility of contrast-enhanced diffuse optical mammography in humans has been shown by Ntziachristos et al.<sup>35</sup> Combining this imaging technique with target-specific fluorochromes as described in this work should greatly enhance the diagnostic accuracy for detecting breast cancer at an early tumor stage.<sup>36</sup> Besides tomographic imaging, planar imaging techniques such as FRI can easily be translated for clinical use. A tumor binding fluorochrome could for instance be applied to preoperatively “tag” the tissue to be resected. The NIR signal deriving from the tumor could then easily be detected with planar optical imaging techniques in the operating room, and thus tumor margins could be visualized for the surgeon.<sup>37,38</sup>

In conclusion, our study shows that CD13/APN expression can be imaged *in vivo* using fluorescence reflectance imaging and fluorescence-mediated tomography approaches. Since FMT allowed 3-D reconstruction of fluorochrome distribution, the tumor-to-background ratio could be significantly enhanced and furthermore quantified noninvasively. This imaging technique is therefore a versatile tool not only for experimental small animal molecular imaging but potentially also for noninvasive target detection, e.g., in clinical breast cancer imaging.<sup>36</sup>

### Acknowledgments

We thank Wiebke Gottschlich, Ingrid Otto-Valk, Ursula Römer, and Janine Ring for technical assistance. For critical reading and fruitful discussion, we gratefully thank Prof. Dr. Werner Schlegel (University of Münster, Germany). This work was supported in part by the Deutsche Forschungsgemeinschaft (DFG) (BR 1653/2-1, SFB 656 Project A4) and the European Community (IP 6th framework; LSHG-CT-2003-503259).

### References

1. C. Bremer, V. Ntziachristos, and R. Weissleder, “Optical-based molecular imaging: contrast agents and potential medical applications,” *Eur. Radiol.* **13**(2), 231–243 (2003).
2. J. Grimm, D. G. Kirsch, S. D. Windsor, C. F. Kim, P. M. Santiago, V. Ntziachristos, T. Jacks, and R. Weissleder, “Use of gene expression profiling to direct *in vivo* molecular imaging of lung cancer,” *Proc. Natl. Acad. Sci. U.S.A.* **102**(40), 14404–14409 (2005).
3. U. Mahmood and R. Weissleder, “Near-infrared optical imaging of proteases in cancer,” *Mol. Cancer Ther.* **2**(5), 489–496 (2003).
4. V. Ntziachristos, C. Bremer, and R. Weissleder, “Fluorescence imaging with near-infrared light: new technological advances that enable *in vivo* molecular imaging,” *Eur. Radiol.* **13**(1), 195–208 (2003).
5. E. E. Graves, D. Yessayan, G. Turner, R. Weissleder, and V. Ntziachristos, “Validation of *in vivo* fluorochrome concentrations measured using fluorescence molecular tomography,” *J. Biomed. Opt.* **10**(4), 44019 (2005).
6. X. Montet, V. Ntziachristos, J. Grimm, and R. Weissleder, “Tomographic fluorescence mapping of tumor targets,” *Cancer Res.* **65**(14), 6330–6336 (2005).
7. V. Ntziachristos, C. Bremer, E. E. Graves, J. Ripoll, and R. Weissleder, “*In vivo* tomographic imaging of near-infrared fluorescent probes,” *Mol. Imaging* **1**(2), 82–88 (2002).
8. V. Ntziachristos, C. Bremer, C. Tung, and R. Weissleder, “Imaging cathepsin B up-regulation in HT-1080 tumor models using fluorescence-mediated molecular tomography (FMT),” *Acad. Radiol.* **9**, Suppl 2, S323–325 (2002).
9. V. Ntziachristos, C. H. Tung, C. Bremer, and R. Weissleder, “Fluorescence molecular tomography resolves protease activity *in vivo*,” *Nat. Med.* **8**(7), 757–760 (2002).
10. D. Riemann, A. Kehlen, and J. Langner, “CD13—not just a marker in leukemia typing,” *Immunol. Today* **20**(2), 83–88 (1999).
11. S. V. Bhagwat, J. Lahdenranta, R. Giordano, W. Arap, R. Pasqualini, and L. H. Shapiro, “CD13/APN is activated by angiogenic signals and is essential for capillary tube formation,” *Blood* **97**(3), 652–659 (2001).
12. R. Pasqualini, E. Koivunen, R. Kain, J. Lahdenranta, M. Sakamoto, A. Stryhn, R. A. Ashmun, L. H. Shapiro, W. Arap, and E. Ruoslahti, “Aminopeptidase N is a receptor for tumor-homing peptides and a target for inhibiting angiogenesis,” *Cancer Res.* **60**(3), 722–727 (2000).
13. Y. Sato, “Role of aminopeptidase in angiogenesis,” *Biol. Pharm. Bull.* **27**(6), 772–776 (2004).
14. W. Arap, R. Pasqualini, and E. Ruoslahti, “Cancer treatment by targeted drug delivery to tumor vasculature in a mouse model,” *Science* **279**(5349), 377–380 (1998).
15. G. Colombo, F. Curnis, G. M. De Mori, A. Gasparri, C. Longoni, A. Sacchi, R. Longhi, and A. Corti, “Structure-activity relationships of linear and cyclic peptides containing the **NGR** tumor-homing motif,” *J. Biol. Chem.* **277**(49), 47891–47897 (2002).
16. Y. van Hensbergen, H. J. Broxterman, Y. W. Elderkamp, J. Lankelma, J. C. Beers, M. Heijn, E. Boven, K. Hoekman, and H. M. Pinedo, “A doxorubicin-CNGRC-peptide conjugate with prodrug properties,” *Biochem. Pharmacol.* **63**(5), 897–908 (2002).
17. Z. Zhang, H. Harada, K. Tanabe, H. Hatta, M. Hiraoka, and S. I. Nishimoto, “Aminopeptidase N/CD13 targeting fluorescent probes: synthesis and application to tumor cell imaging,” *Peptides* **26**(11), 2182–2187 (2005).
18. Z. Zhang, H. Hatta, K. Tanabe, and S. Nishimoto, “A new class of 5-fluoro-2'-deoxyuridine prodrugs conjugated with a tumor-homing cyclic peptide CNGRC by ester linkers: synthesis, reactivity, and tumor-cell-selective cytotoxicity,” *Pharm. Res.* **22**(3), 381–389 (2005).
19. F. Pastorino, C. Brignole, D. Marimpetri, M. Cilli, C. Gambini, D. Ribatti, R. Longhi, T. M. Allen, A. Corti, and M. Ponzoni, “Vascular damage and anti-angiogenic effects of tumor vessel-targeted liposomal chemotherapy,” *Cancer Res.* **63**(21), 7400–7409 (2003).
20. A. Corti and M. Ponzoni, “Tumor vascular targeting with tumor necrosis factor alpha and chemotherapeutic drugs,” *Ann. N.Y. Acad. Sci.* **1028**, 104–112 (2004).
21. Y. van Hensbergen, H. J. Broxterman, R. Hanemaaijer, A. S. Jorna, N. A. van Lent, H. M. Verheul, H. M. Pinedo, and K. Hoekman, “Soluble aminopeptidase N/CD13 in malignant and nonmalignant effusions and intratumoral fluid,” *Clin. Cancer Res.* **8**(12), 3747–3754 (2002).
22. V. Ntziachristos, J. Ripoll, L. V. Wang, and R. Weissleder, “Looking and listening to light: the evolution of whole-body photonic imaging,” *Nat. Biotechnol.* **23**(3), 313–320 (2005).
23. Y. van Hensbergen, H. J. Broxterman, S. Rana, P. J. van Diest, M. C. Duyndam, K. Hoekman, H. M. Pinedo, and E. Boven, “Reduced growth, increased vascular area, and reduced response to cisplatin in CD13-overexpressing human ovarian cancer xenografts,” *Clin. Cancer Res.* **10**(3), 1180–1191 (2004).

24. F. Curnis, G. Arrigoni, A. Sacchi, L. Fischetti, W. Arap, R. Pasqualini, and A. Corti, "Differential binding of drugs containing the **NGR** motif to CD13 isoforms in tumor vessels, epithelia, and myeloid cells," *Cancer Res.* **62**(3), 867–874 (2002).
25. Y. Yokoyama and S. Ramakrishnan, "Addition of an aminopeptidase N-binding sequence to human endostatin improves inhibition of ovarian carcinoma growth," *Cancer* **104**(2), 321–331 (2005).
26. A. Dirksen, S. Langereis, B. F. de Waal, M. H. van Genderen, E. W. Meijer, Q. G. de Lussanet, and T. M. Hackeng, "Design and synthesis of a bimodal target-specific contrast agent for angiogenesis," *Org. Lett.* **6**(26), 4857–4860 (2004).
27. K. Licha, B. Riefke, V. Ntziachristos, A. Becker, B. Chance, and W. Semmler, "Hydrophilic cyanine dyes as contrast agents for near-infrared tumor imaging: synthesis, photophysical properties, and spectroscopic *in vivo* characterization," *Photochem. Photobiol.* **72**(3), 392–398 (2000).
28. D. Bordessoule, M. Jones, K. C. Gatter, and D. Y. Mason, "Immunohistological patterns of myeloid antigens: tissue distribution of CD13, CD14, CD16, CD31, CD36, CD65, CD66, and CD67," *Br. J. Haematol.* **83**(3), 370–383 (1993).
29. J. Dixon, L. Kaklamanis, H. Turley, I. D. Hickson, R. D. Leek, A. L. Harris, and K. C. Gatter, "Expression of aminopeptidase-n (CD 13) in normal tissues and malignant neoplasms of epithelial and lymphoid origin," *J. Clin. Pathol.* **47**(1), 43–47 (1994).
30. R. Haubner and H. J. Wester, "Radiolabeled tracers for imaging of tumor angiogenesis and evaluation of anti-angiogenic therapies," *Curr. Pharm. Des.* **10**(13), 1439–1455 (2004).
31. R. Haubner, H. J. Wester, F. Burkhart, R. Senekowitsch-Schmidtke, W. Weber, S. L. Goodman, H. Kessler, and M. Schwaiger, "Glycosylated RGD-containing peptides: tracer for tumor targeting and angiogenesis imaging with improved biokinetics," *J. Nucl. Med.* **42**(2), 326–336 (2001).
32. R. Haubner, H. J. Wester, U. Reuning, R. Senekowitsch-Schmidtke, B. Diefenbach, H. Kessler, G. Stocklin, and M. Schwaiger, "Radio-labeled alpha(v)beta3 integrin antagonists: a new class of tracers for tumor targeting," *J. Nucl. Med.* **40**(6), 1061–1071 (1999).
33. X. Chen, M. Tohme, R. Park, Y. Hou, J. R. Bading, and P. S. Conti, "Micro-PET imaging of alphavbeta3-integrin expression with 18F-labeled dimeric RGD peptide," *Mol. Imaging* **3**(2), 96–104 (2004).
34. Z. Cheng, Y. Wu, Z. Xiong, S. S. Gambhir, and X. Chen, "Near-infrared fluorescent RGD peptides for optical imaging of integrin alphavbeta3 expression in living mice," *Bioconjugate Chem.* **16**(6), 1433–1441 (2005).
35. V. Ntziachristos, A. G. Yodh, M. Schnall, and B. Chance, "Concurrent MRI and diffuse optical tomography of breast after indocyanine green enhancement," *Proc. Natl. Acad. Sci. U.S.A.* **97**(6), 2767–2772 (2000).
36. J. M. Martinez, I. Prieto, M. J. Ramirez, C. Cueva, F. Alba, and M. Ramirez, "Aminopeptidase activities in breast cancer tissue," *Clin. Chem.* **45**(10), 1797–1802 (1999).
37. M. F. Kircher, U. Mahmood, R. S. King, R. Weissleder, and L. Josephson, "A multimodal nanoparticle for preoperative magnetic resonance imaging and intraoperative optical brain tumor delineation," *Cancer Res.* **63**(23), 8122–8125 (2003).
38. A. M. De Grand and J. V. Frangioni, "An operational near-infrared fluorescence imaging system prototype for large animal surgery," *Technol. Cancer Res. Treat.* **2**(6), 553–562 (2003).